






## Insight of mixed convective heat transport in molybdenum disulfide-water nanofluid flow on moving vertical permeable plate with homogeneous-heterogeneous reactions

Amit Kumar Pandey\*, Momtaz Begum†, Sohita Rajput <sup>\*,†,§</sup>,  
Krishnendu Bhattacharyya <sup>\*,||,\*\*</sup>, Mitu Dular <sup>\*</sup>, Astick Banerjee <sup>†</sup>  
and Ali J. Chamkha <sup>§</sup>

*\*Department of Mathematics, Institute of Science,  
Banaras Hindu University, Varanasi 221005,  
Uttar Pradesh, India*

*†Department of Computer Science and Engineering,  
Prime University, Mirpur-1, Dhaka, Bangladesh*

*‡Department of Mathematics, Sidho-Kanho-Birsha University,  
Purulia 723104, West Bengal, India*

*§Faculty of Engineering, Kuwait College of Science and Technology,  
Doha District, Kuwait  
✉sohita.math@gmail.com  
||krishmath@bhu.ac.in*

Received 19 June 2023

Revised 15 October 2023

Accepted 1 November 2023

Published 2 February 2024

This analysis is framed to take care of the high heat transfer demand from various application prospects and in this context nanofluid may be in consideration because nanofluids are well-known liquids with higher heat transfer capabilities. Here, a mixed convection flow of Molybdenum disulfide-water ( $\text{MoS}_2\text{-H}_2\text{O}$ ) nanofluid on a moving vertical plate is examined when there are chemical reactions. Nanofluid problem is investigated using Tiwari and Das model, and numerically solved by “bvp4c” method. For the considered effects in the study, overshoots in temperature profile of nanofluid are observed. Momentum and thermal layer thicknesses become thinner with suction and thicker with blowing. Temperature overshoot is higher for blowing cases. Enhanced homogeneous–heterogeneous reactions lead to rise of the concentration boundary layer’s thickness. Also, magnitude of surface-drag force decays and cooling rate enhances with  $\text{MoS}_2\text{-H}_2\text{O}$  nanofluid mixed convection. For weaker suction and for blowing, cooling of nanofluid is faster with larger volume fraction of nanoparticles, but contrast results are obtained for greater suction. Importantly, compared to the homogeneous reaction, the heterogeneous reaction exhibits more impactful influences on flow and heat-mass transport characters.

*Keywords:* Mixed convection; Molybdenum disulfide-water nanofluid; moving vertical permeable plate; homogenous–heterogeneous reactions.

\*\*Corresponding authors.

## 1. Introduction

A primary industrial need is for the cooling of electrical equipment, and because typical fluids have weak heat transfer properties, they are unable to meet the required need due to their low thermal conductive nature. Thermal conductivities of many classical fluids, like water, ethylene glycol and engine oil. can be enriched by suspending nanometer-sized solid particles of metals, nitrides, carbides, oxides and carbon-nanotubes in base fluids. Additionally, this particular combination is known as a nanofluid. Choi<sup>1</sup> introduced the term “nanofluid”. Due to their superior wetting and spreading behavior, nanofluids are also vital for formation of nanostructured materials for engineering fluids with critical properties, like oil cleaning from surfaces investigated by Bachok *et al.*<sup>2</sup> In comparison to fluid containing micro- or millimeter-sized particles, the nanofluid’s key feature is the considerable improvement of the thermal and physical characteristics of the base fluid, which includes little obstruction of flow passages, long-term stability, and homogeneity. Tiwari and Das<sup>3</sup> developed a homogeneous model for nanofluid analysis. In various technical and industrial issues, including transportation, cooling of electronic equipment, solar water heating, grain storage installations, chemical catalytic reactors and drug diffusion in blood veins, the present advancement of heat transfer nanofluid is crucial. Makinde and Aziz<sup>4</sup> looked into the heat transmission and flow on a stretched sheet with convective boundary condition (CBC) for a nanofluid. Das<sup>5</sup> explored the combined convective flow approaching toward stagnation point with heat transport of Cu-water nanofluid on contracting sheet. Acharya *et al.*<sup>6</sup> examined how copper nanofluid having base as kerosene and water affected the flow between parallel plates when a magnetic field is there in the flow dynamics. The influence of H<sub>2</sub>O-based nanofluids of Cu and Ag across a contracting sheet with CBC was discussed by Das *et al.*<sup>7</sup> using Lie-group approach. Acharya *et al.*<sup>8</sup> looked at the continuous flow of nanofluid having H<sub>2</sub>O-based Ti and Ag-nanoparticles across thin expanding surface. The double solutions for MHD nanofluid flow on power-law expanding/shrinking porous surface with dissipation effect were recently found by Dhanai *et al.*<sup>9</sup> Verma *et al.*<sup>10</sup> studied mixed convective flow of Cu-H<sub>2</sub>O on an expanding surface inside porous material, and also Verma *et al.*<sup>11</sup> performed comparative study between graphene and graphene oxide nanofluid flows over exponential contracting surface inside porous medium. Ibrahim *et al.*<sup>12</sup> deliberated the water-based magnetite nanofluid flow with entropy generation and uniform magnetic field in a circular microtube with twisted porous blocks. Second-grade nanofluid flow taking properties, like thermal conductivity and mass diffusivity being variable with Cattaneo-Christov double diffusion model over a Riga surface was discussed by Chu *et al.*<sup>13</sup> Abbas *et al.*<sup>14</sup> and Ashraf *et al.*<sup>15</sup> examined interesting nanofluid flow problems with mixed convection. Hybrid nanofluid (AA7072-AA7075-water) flow over curved expanding surface by using non-Fourier heat flux model was analyzed by Madhukesh *et al.*<sup>16</sup> Unsteady hybrid nanofluid flow past a shrinking sheet with partial slip condition and stability analysis was inspected by Lund *et al.*<sup>17</sup>

Molybdenum disulphide ( $\text{MoS}_2$ ) is a 2D-layered inorganic nanomaterial with numerous unique properties, including low cost, substantial surface area and minimal cytotoxicity. Molybdenum disulfide has exceptional chemical as well as thermal stability. Molybdenum disulfide nanoparticles possess excellent physical qualities, like a low coefficient of friction and strong catalytic activity. In comparison to the bulk material, they also have more active surface area, and also have a higher adsorption capacity. Hamid *et al.*<sup>18</sup> exhibited effect of  $\text{MoS}_2$ -nanoparticle's shape on rotating nanofluid flow having variable thermal conductivity along expanding surface. Samadder *et al.*<sup>19</sup> derived the similarity solution for free convective nanofluid ( $\text{MoS}_2\text{-H}_2\text{O}$ ) flow inside a square cavity. Hybrid nanofluid ( $\text{Go-MoS}_2/\text{H}_2\text{O}$ ) flow having thermal radiation and joule heating on a contracting cylinder was investigated by Narayanaswamy *et al.*<sup>20</sup>

Allied sectors and chemical engineering are using chemical processes in a variety of applications. When components are involved in chemical reactions that are occurring at the same or different phases, it remains important to focus on heat flow. The processes of combustion, catalysis and biochemical systems are only a few examples of chemically reactive systems that combine homogeneous and heterogeneous reactions. In contrast to heterogeneous reactions, which occur in two or more phases, homogeneous reactions take place in single phase and are represented by cubic autocatalysis. This is the key distinction between homogeneous and heterogeneous reactions. The interesting characters of isothermal homogeneous–heterogeneous reactions in viscous flow inside boundary layer on flat plate were explored by Merkin<sup>21</sup>. Nanofluid flow across expanding porous surface having homogeneous–heterogeneous reactions was closely inspected by Kameswaran *et al.*<sup>22</sup> Joint effects of heat production and MHD character on nanofluid flow past stretched surface containing chemical reactions (homogeneous–heterogeneous) were described by Nandkeolyar *et al.*<sup>23</sup> Das *et al.*<sup>24</sup> scrutinized the mixed convective nanofluid flow approaching toward a stagnation point on stretched sheet having homogeneous–heterogeneous reactions. Ramzan *et al.*<sup>25</sup> explored the aspects of hybrid nanofluid  $\text{Ni-ZnFe}_2\text{O}_4/\text{water}$  flow on curved stretching surface with thermal radiation, chemical reaction and slip condition and concluded that concentration decays with both chemical reaction parameters. Some recent investigations on flow having heterogeneous–homogeneous reactions in different physical scenarios were studied by Hayat *et al.*,<sup>26</sup> Zaib *et al.*,<sup>27</sup> Sravanthi *et al.*<sup>28</sup> and Abbas *et al.*<sup>29</sup>

Motivated by the superior and exciting thermophysical characters of  $\text{MoS}_2$ -nanoparticles along with their effects on the characteristics of heterogeneous–homogeneous chemical processes and how those nanoparticles affect the dynamics of mixed convection flow with exploration of possibilities of industrial and engineering applications, the existing study focuses on the impact of mixed convection of the  $\text{MoS}_2$ -water nanoliquid with homogeneous–heterogeneous chemical reactions on vertically moving flat plate. Well-known Tiwari and Das<sup>3</sup> model is adopted to simulate the nanofluid flow. Further, some suitable transformations are considered to transform flow governing nonlinear PDEs into ODEs. Finally, the solutions of the

reduced ODEs are obtained via numerical method, “bvp4c”, MATLAB-based scheme and accuracy of the computed values is ensured by validating them with previous findings in literature. Noticeable impacts of flow influencing parameters are drawn via graphical approach.

The whole paper is organized in such a manner that Sec. 1 presents the necessary background, in which related studies of the proposed work are described. In Sec. 2, the current problem with governing equations and boundary condition is discussed and equations are transformed into ODEs by using suitable transformations. In Sec. 3, the numerical method is described by which the problem is solved. Obtained results and their graphical discussion are presented in Sec. 4. Finally, important remarks of the overall study are mentioned in Sec. 5 followed by the bibliography.

## 2. Formulation and Basic Equations

Consider a mixed convective heat transport in MoS<sub>2</sub>-water nanofluid flow over moving vertical plate with homogenous–heterogeneous reactions. Geometry along with flow model has been depicted in Fig. 1. In this problem, vertical surface is taken over which fluid is flowing. Therefore, “*x*”-coordinate which is the stream coordinate is considered along the surface, i.e. vertical and “*y*”-coordinate perpendicular to the surface, i.e. horizontal. Physical sketch of considered model is divided into two portions, i.e. assisting and opposing flow regions because of two possible plate velocity directions, it may be upward or downward and flow behavior is different in both possibilities. Taking the description of Chaudhary and Merkin,<sup>30</sup> the isothermal homogeneous–heterogeneous reactions model may be stated as



while  $A \rightarrow B$ , rate =  $k_p C_A^*$  gives the 1st order isothermal single reaction.

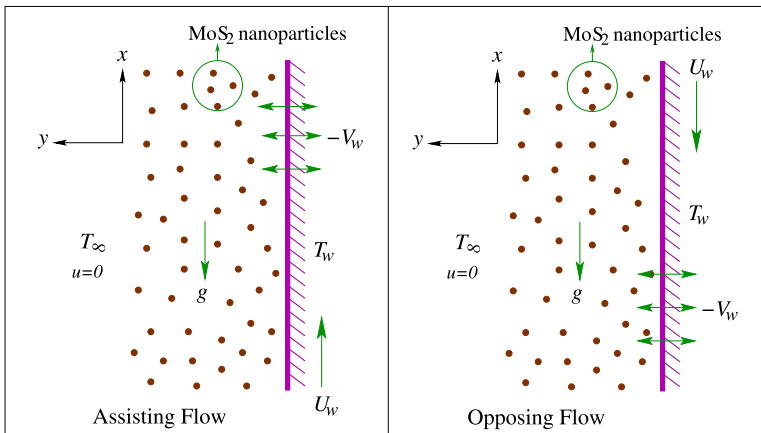


Fig. 1. (Color online) Geometry along with the flow model of examined problem.

Here  $C_A^*$  and  $C_B^*$  are chemical species concentrations of  $A$  and  $B$ , whereas  $k_c$  and  $k_p$  represent constants. Using Tiwari–Das model,<sup>3</sup> the basic boundary layer equations which govern flow, heat and species transports may be specified as<sup>27,28</sup>

$$\frac{\partial u}{\partial x} + \frac{\partial v}{\partial y} = 0, \tag{2}$$

$$u \frac{\partial u}{\partial x} + v \frac{\partial u}{\partial y} = \frac{\mu_{nf}}{\rho_{nf}} \frac{\partial^2 u}{\partial y^2} + \frac{(\rho\beta)_{nf}}{\rho_{nf}} g(T - T_\infty), \tag{3}$$

$$u \frac{\partial T}{\partial x} + v \frac{\partial T}{\partial y} = \frac{\kappa_{nf}}{(\rho c_p)_{nf}} \frac{\partial^2 T}{\partial y^2}, \tag{4}$$

$$u \frac{\partial C_A^*}{\partial x} + v \frac{\partial C_A^*}{\partial y} = D_A \frac{\partial^2 C_A^*}{\partial y^2} - k_c C_A^* C_B^{*2}, \tag{5}$$

$$u \frac{\partial C_B^*}{\partial x} + v \frac{\partial C_B^*}{\partial y} = D_B \frac{\partial^2 C_B^*}{\partial y^2} + k_c C_A^* C_B^{*2}. \tag{6}$$

The boundary conditions are

$$\left. \begin{aligned} u = U_w, \quad v = -v_w, \quad T = T_w(x), \quad D_A \frac{\partial C_A^*}{\partial y} = k_p C_A^*, \\ D_B \frac{\partial C_B^*}{\partial y} = -k_p C_A^* \quad \text{at } y = 0, \\ u \rightarrow 0, \quad T \rightarrow T_\infty, \quad C_A^* \rightarrow C_{A0}^*, \quad C_B^* \rightarrow 0 \quad \text{as } y \rightarrow \infty, \end{aligned} \right\} \tag{7}$$

where  $u$  and  $v$  are velocity components, respectively, in  $x$  and  $y$  directions,  $T$  denotes the temperature,  $T_\infty$  gives free stream temperature,  $T_w$  signifies wall temperature given by  $T_w(x) = T_\infty + T_0(L/x)$  ( $T_0$  is reference temperature and  $L$  is characteristics length),  $D_A$  and  $D_B$  indicate species diffusion coefficients for species  $A$  and  $B$ , respectively,  $C_{A0}^* > 0$  denotes a constant,  $v_w = V_0(\sqrt{L/x})$  gives variable suction/injection velocity,  $g$  states gravitational acceleration. Here  $\rho_{nf}$ ,  $(\rho c_p)_{nf}$ ,  $\mu_{nf}$ ,  $\beta_{nf}$ ,  $\kappa_{nf}$  are density, specific heat capacitance, viscosity, thermal expansion coefficients, thermal conductivity of nanofluid, respectively, which are defined as

$$\left. \begin{aligned} \rho_{nf} = (1 - \phi)\rho_f + \phi\rho_s, \quad (\rho c_p)_{nf} = (1 - \phi)(\rho c_p)_f + \phi(\rho c_p)_s, \quad \mu_{nf} = \frac{\mu_f}{(1 - \phi)^{2.5}}, \\ (\rho\beta)_{nf} = (1 - \phi)(\rho\beta)_f + \phi(\rho\beta)_s, \quad \frac{\kappa_{nf}}{\kappa_f} = \frac{(\kappa_s + 2\kappa_f) - 2\phi(\kappa_f - \kappa_s)}{(\kappa_s + 2\kappa_f) + \phi(\kappa_f - \kappa_s)}. \end{aligned} \right\} \tag{8}$$

Here  $\phi$  is solid volume fraction of nanoparticle,  $\kappa_f$ ,  $\rho_f$ ,  $\beta_f$  are thermal conductivity, density, thermal expansion coefficient of base fluid and  $\kappa_s$ ,  $\rho_s$ ,  $\beta_s$  are thermal conductivity, density, thermal expansion coefficient of nanosized solid

Table 1. Thermophysical properties of MoS<sub>2</sub>-water nanofluid.<sup>19</sup>

Property	Water	MoS <sub>2</sub> nanoparticle
$C_p$	4179	397.21
$\rho$	997	$5.06 \times 10^3$
$\kappa$	0.613	904.4
$\beta$	$210 \times 10^{-6}$	$2.8424 \times 10^{-5}$

particles. Here, MoS<sub>2</sub> is considered as nanoparticle along with H<sub>2</sub>O as base fluid. Thermal properties of MoS<sub>2</sub> nanoparticle and H<sub>2</sub>O are given in Table 1.

Now, the following transformations have been introduced<sup>28</sup>:

$$\eta = y \sqrt{\frac{U_w}{2\nu_f x}}, \quad \psi = \sqrt{2U_w \nu_f x} f(\eta), \quad g(\eta) = \frac{C_A^*}{C_{A0}^*}, \quad (9)$$

$$h(\eta) = \frac{C_B^*}{C_{A0}^*}, \quad \theta(\eta) = \frac{T - T_\infty}{T_w - T_\infty},$$

where  $\eta$  and  $\nu_f$  are a variable and base fluid kinematic viscosity, respectively, and  $\psi$  represents stream function stated as:  $u = \frac{\partial \psi}{\partial y}$  and  $v = -\frac{\partial \psi}{\partial x}$ .

In view of relation (9), Eqs. (3)–(6) are transformed into the following ODEs:

$$\frac{1}{(1 - \phi)^{2.5}(1 - \phi + \phi \frac{\rho_s}{\rho_f})} f''' + f f'' + \lambda \left( \frac{1 - \phi + \phi \frac{(\rho\beta)_s}{(\rho\beta)_f}}{1 - \phi + \phi \frac{\rho_s}{\rho_f}} \right) \theta = 0, \quad (10)$$

$$\frac{\kappa_{nf}}{\kappa_f} \frac{\theta''}{2} + \text{Pr} \left[ 1 - \phi + \phi \frac{(\rho c_p)_s}{(\rho c_p)_f} \right] \left( \frac{1}{2} f \theta' + f' \theta \right) = 0, \quad (11)$$

$$\frac{1}{\text{Sc}} g'' + f g' - K g h^2 = 0, \quad (12)$$

$$\frac{\delta}{\text{Sc}} h'' + f h' + K g h^2 = 0, \quad (13)$$

subject to

$$\left. \begin{aligned} f(0) = S, \quad f'(0) = 1, \quad \theta(0) = 1, \quad g'(0) = K_p g(0), \quad \delta h'(0) = -K_p g(0), \\ f'(\infty) \rightarrow 0, \quad \theta(\infty) \rightarrow 0, \quad g(\infty) \rightarrow 1, \quad h(\infty) \rightarrow 0, \end{aligned} \right\} \quad (14)$$

where prime indicates derivative with respect to  $\eta$ ,  $\text{Pr} = \nu_f(\rho c_p)_f / \kappa_f$  is Prandtl number,  $\lambda = 2\beta_f g T_0 L / U_w^2$  is mixed convection parameter,  $K = 2x k_c C_{A0}^{*2} / U_w$  gives homogenous reaction parameter describing its strength,  $K_p = (k_p / D_A) \sqrt{2x \nu_f / U_w}$  is heterogeneous reaction parameter which gives measurement of strength,  $\text{Sc} = \nu_f / D_A$  is Schmidt number,  $\delta = D_B / D_A$  denotes ratio of mass diffusion coefficients, and

Table 2. List of important involved physical parameters.

Parameters	Physical significance
Pr	Ratio of momentum and heat transports
$\lambda$	Signifies the impact of natural convection along with forced convection
$K$	A localised dimensionless parameter for homogenous reaction
$K_p$	A localised dimensionless parameter for heterogeneous reaction
Sc	Ratio of momentum diffusivity to mass diffusivity of species A
$\delta$	Ratio of mass diffusion coefficients of species A and B

$S = V_0 \sqrt{2L/U_w v_f}$  is suction/injection parameter (positive value of  $S$  gives suction, whereas negative value of  $S$  yields injection). Important parameters along with their physical significance are listed in Table 2.

Moreover, it is also supposed that chemical species A and B are of analogous size. To further convince, assume that diffusion coefficients  $D_A$  and  $D_B$  are equal, i.e.  $\delta = 1^{28}$  and hence

$$g(\eta) + h(\eta) = 1. \tag{15}$$

Above statement indicates reformation of Eqs. (12) and (13) as

$$\frac{1}{Sc} g'' + fg' - Kg(1-g)^2 = 0, \tag{16}$$

with

$$g'(0) = K_p g(0), \quad g(\infty) \rightarrow 1. \tag{17}$$

Measurements having industrial interests are skin-friction coefficient and Nusselt number, those are connected to  $f''(0)$  and  $-\theta'(0)$  and expressions of these quantities are given by

$$\begin{aligned} (2Re_x)^{1/2} C_{fx} &= \frac{\mu_{nf}}{\mu_f} f''(0) = \frac{1}{(1-\phi)^{2.5}} f''(0) \quad \text{and} \\ (Re_x/2)^{-1/2} Nu_x &= -\frac{\kappa_{nf}}{\kappa_f} \theta'(0), \end{aligned} \tag{18}$$

where  $Re_x = xU_w/v_f$  is local Reynolds number.

### 3. Solution Technique

The numerical method, the MATLAB programme “bvp4c”<sup>31-35</sup> is solved in Eqs. (10), (11) and (16), together with the boundary conditions stated in Eqs. (14) and (17). This numerical method begins by altering boundary value problem (BVP) to a problem of initial value (IVP), from which an ODE of 1st-order system is derived. We examine our answer for various  $\eta_\infty$ , until we obtain an asymptotically convergent solution that meets the required tolerance level.

In our comprehensive study, we take the value of  $\eta_\infty = 10$  and integrate the first-order system provided by

$$\begin{aligned}
 f' &= z'_1 = z_2, & z'_2 &= z_3, & \theta &= z_4, & z'_4 &= z_5, & g &= z_6, & z'_6 &= z_7, \\
 z'_3 &= \left( (1 - \phi)^{2.5} \left( 1 - \phi + \phi \frac{\rho_s}{\rho_f} \right) \right) \left\{ -z_1 z_3 - \lambda \left( \frac{1 - \phi + \phi \frac{(\rho\beta)_s}{(\rho\beta)_f}}{1 - \phi + \phi \frac{\rho_s}{\rho_f}} \right) z_4 \right\}, \\
 z'_5 &= -\frac{2}{(k_{n,f}/k_f)} \Pr \left[ 1 - \phi + \phi \frac{(\rho c_p)_s}{(\rho c_p)_f} \right] \left( \frac{1}{2} z_1 z_5 + z_2 z_4 \right), \\
 z'_7 &= \text{Sc} \{ -z_1 z_7 + K z_6 (1 - z_6)^2 \},
 \end{aligned}$$

with boundary restrictions given by

$$\left. \begin{aligned}
 z_1(0) &= S, & z_2(0) &= 1, & z_4(0) &= 1, & z_7(0) &= K_p z_6(0), \\
 z_2(\infty) &\rightarrow 0, & z_4(\infty) &\rightarrow 0, & z_6(\infty) &\rightarrow 1.
 \end{aligned} \right\}$$

#### 4. Results and Essential Discussion

The outcomes are assessed for various parameter values which are arising from the system of transported equations and the findings are presented graphically. For all computations and visualizations, the default values for the parameters are  $\lambda = 0.1$ ,  $\phi = 0.02$ ,  $S = 0.2$ ,  $\text{Pr} = 6.13$ ,  $\text{Sc} = 1$ ,  $K = 0.4$ ,  $K_p = 0.4$ , when those are not varied. Table 3 depicts the comparative values of  $-\theta'(0)/\sqrt{2}$  obtained by present computation and by Mohamed *et al.*<sup>36</sup> and Sravanthi *et al.*<sup>28</sup> for various Pr and those are exhibiting a brilliant agreement.

Figures 2 and 3 describe the variations in temperature and velocity patterns for different MoS<sub>2</sub>-nanoparticle volume fractions, where  $\phi = 0$  stands for the ordinary fluid. These figures illustrate that flow velocity and momentum boundary layer (MBL) thickness decline with growing  $\phi$ , whereas thermal boundary layer (TBL) thickness increases. Physically, rise in the nanoparticles volume fraction puts

Table 3. Comparative data of  $-\theta'(0)/\sqrt{2}$  for constant wall temperature and boundary conditions  $f(0) = S$ ,  $f'(0) = 0$ ,  $f'(\infty) \rightarrow 1$ , when  $\phi = S = \lambda = 0$ , for different Pr.

Pr	Mohamed <i>et al.</i> <sup>36</sup>	Sravanthi <i>et al.</i> <sup>28</sup>	Present results
0.7	0.292680	0.292676	0.29268032
0.8	0.306917	0.306913	0.30691698
1	0.332057	0.332053	0.33205747
5	0.576689	0.576682	0.57668912
10	0.728141	0.728132	0.72814131
20	—	0.918391	0.91840137

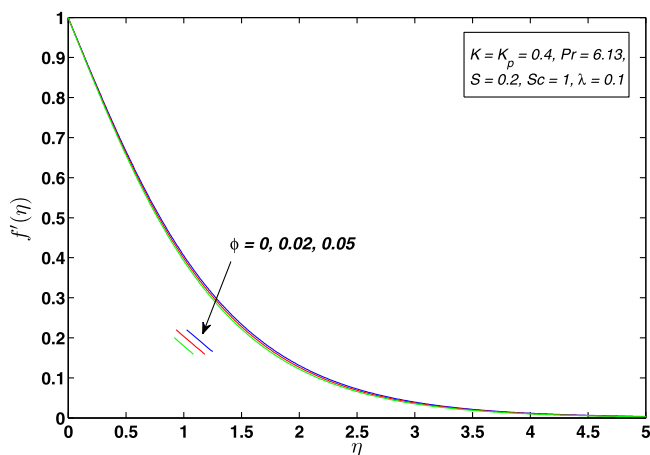


Fig. 2. (Color online) Impact of  $\phi$  on velocity.

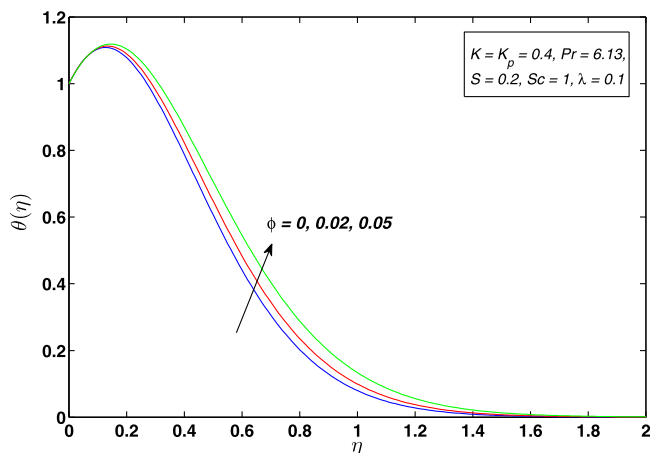


Fig. 3. (Color online) Impact of  $\phi$  on temperature.

restrictions on the convection phenomenon of nanofluid and causes a reduction in velocity. On the other hand, a greater amount of nanoparticle concentration is better for a temperature distribution to develop. Since adding more nanoparticles to a regular fluid increases its ability to transmit heat, accordingly, enlargement of temperature distribution is witnessed. These findings have uses in insulating heat exchange medium and cooling nuclear reactors.

Figure 4 demonstrates that when value of mixed convection parameter ( $\lambda$ ) rises, velocity also upsurges near the plate, i.e. with rising nature of aiding flows ( $\lambda > 0$ ) and it is falling for opposing flows ( $\lambda < 0$ ), but reverse nature is obtained after some distance from the plate. Physically, for positive  $\lambda$ , a favorable pressure gradient is

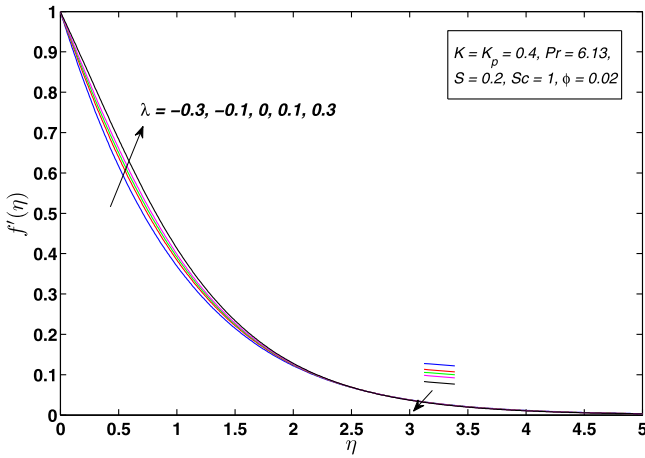


Fig. 4. (Color online) Impact of  $\lambda$  on velocity.

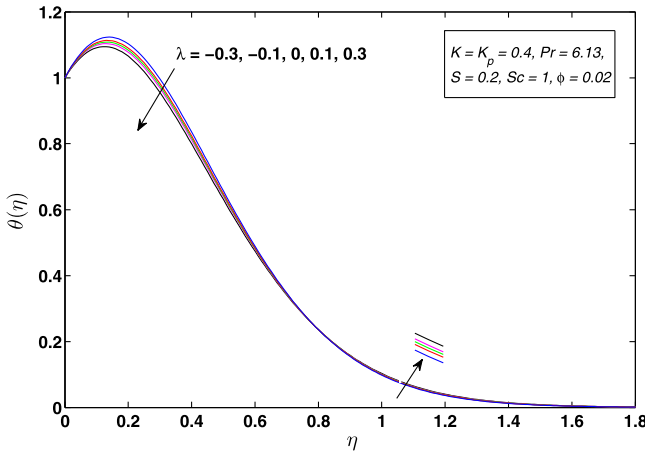


Fig. 5. (Color online) Impact of  $\lambda$  on temperature.

created and it accelerates the fluid motion, whereas for negative  $\lambda$ , the scenario is reverse. Temperature for some values of the mixed convection parameters is presented in Fig. 5. When there is an aiding flow, the temperature near the plate drops with  $\lambda$  and when there is an opposing flow, it displays the opposite pattern, but reversely acts in the region far from the plate. Also, temperature overshoot is observed for mixed convection in aiding flow as well as the opposing flows. Due to the combined impact of natural and forced convection this thermal overshoot is detected.

Figures 6 and 7 display the impact of suction and injection on velocity and temperature. For case of suction, velocity decreases, but reverse nature can be

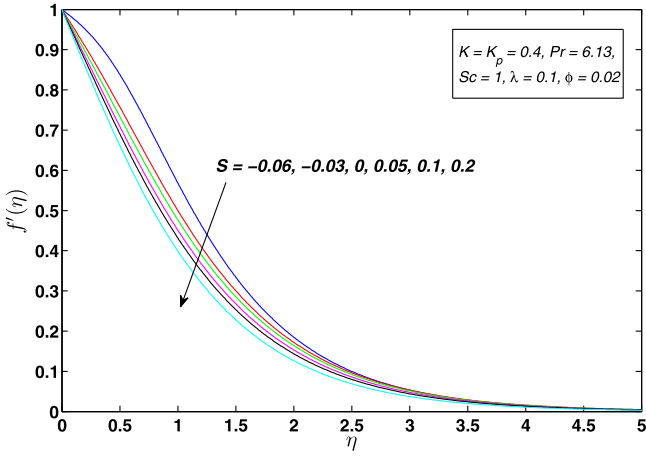


Fig. 6. (Color online) Impact of suction and blowing on velocity.

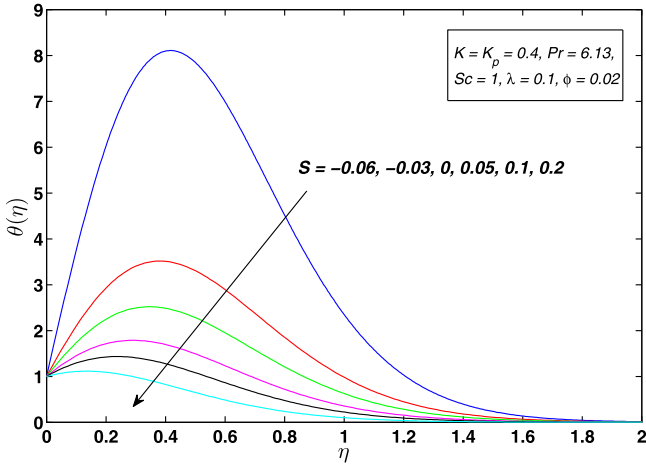


Fig. 7. (Color online) Impact of suction and blowing on temperature.

found in blowing case, i.e. velocity increases. Similar trend is followed by MBL thickness and temperature distribution. This happens because fluid layers near the surface are pulled toward the surface for suction, and pushed away from the surface for injection. Also, a significant temperature overshoot is observed for higher blowing situations.

The variations in velocity and temperature with Prandtl number are presented by Figs. 8 and 9. Both the quantities and their related boundary layer thicknesses reduce with increment in Pr, since higher Prandtl number equates to lower thermal diffusivity. Physically, this signifies that with rise in Pr, the TBL gets

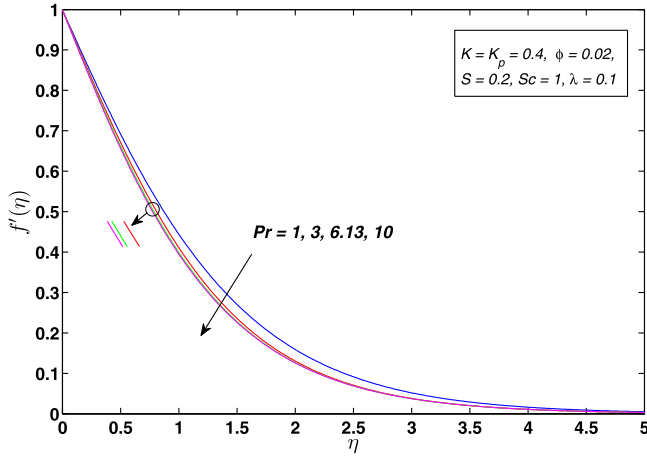


Fig. 8. (Color online) Influence of Pr on velocity for  $\lambda = 0.1$ ,  $\phi = 0.02$ ,  $S = 0.2$ ,  $Sc = 1$ ,  $K = 0.4$ , and  $K_p = 0.4$ .

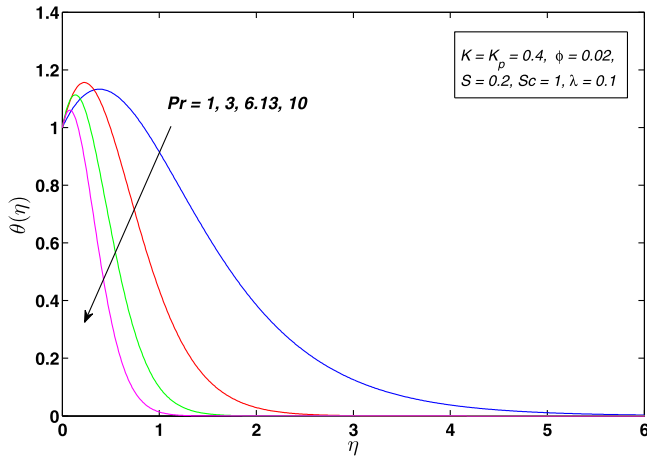


Fig. 9. (Color online) Influence of Pr on temperature for  $\lambda = 0.1$ ,  $\phi = 0.02$ ,  $S = 0.2$ ,  $Sc = 1$ ,  $K = 0.4$ , and  $K_p = 0.4$ .

thinner as ratio of momentum diffusivity to thermal diffusivity is represented by Pr. As a result, rate of cooling in conducting flow may be accelerated using the Prandtl number.

Figures 10–12 are prepared to demonstrate influences of volume fraction of nanoparticle, homogeneous and heterogeneous reaction parameters on concentration. As these parameters increase, concentration decays, while associated layer thickness becomes thicker. The chemical reaction is accelerated by a rise in homogeneous or heterogeneous reaction parameters, which reduces the concentration.

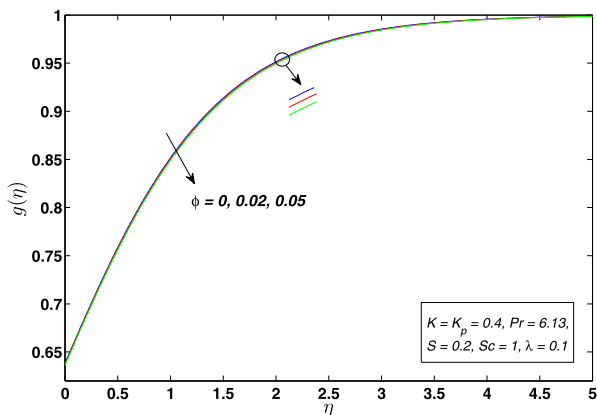


Fig. 10. (Color online) Influence of  $\phi$  on  $g(\eta)$ .

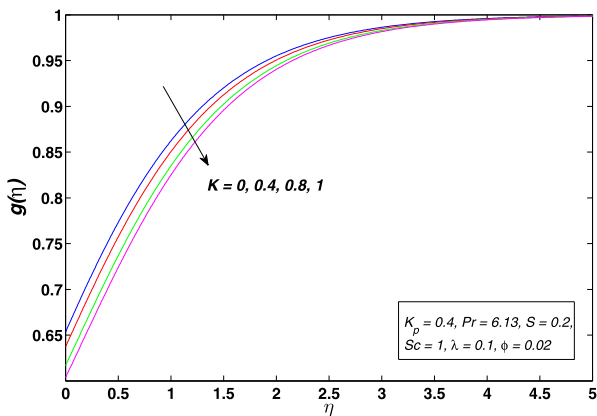


Fig. 11. (Color online) Influence of  $K$  on  $g(\eta)$ .

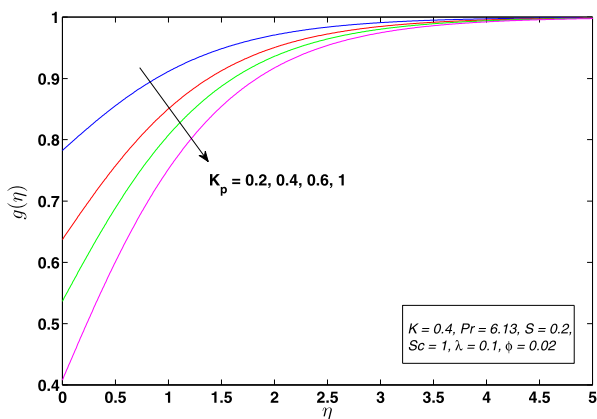


Fig. 12. (Color online) Influence of  $k_p$  on  $g(\eta)$ .

Heterogeneous reaction parameter is more impactful than the homogenous parameter, as shown by the figures.

Influence of mixed convection, suction and blowing for regular fluid and nanofluid ( $\phi = 0.02, 0.05$ ) on surface-drag force along with heat transport rate is illustrated by Figs. 13–16. Comparison between three flowing liquids show that the drag force by the surface on the liquid becomes stronger for large amount of nanoparticles, opposing flow ( $\lambda < 0$ ) and higher suction, while it is weaker for aiding flow ( $\lambda > 0$ ) and blowing cases. This occurs as a result of competing types of forces in aiding as well as opposing flows. Rate of heat transport enhances with higher nanoparticle volume fraction and mixed convection for a specific suction. An interchangeable nature of heat transfer rate is depicted for different volume fractions with suction and

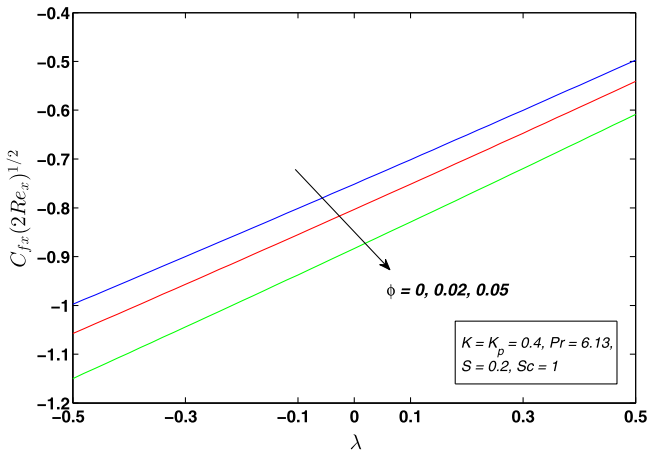


Fig. 13. (Color online) Impacts of  $\phi$  and  $\lambda$  on  $(2Re_x)^{1/2}C_{fx}$ .

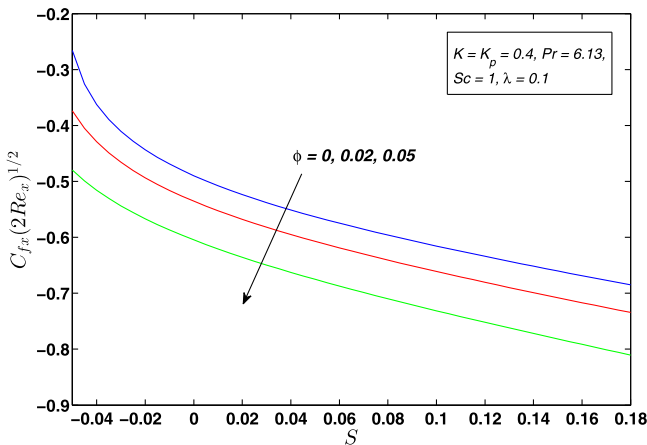


Fig. 14. (Color online) Impacts of  $\phi$  and suction and blowing on  $(2Re_x)^{1/2}C_{fx}$ .

*Insight of mixed convectonal heat transport in molybdenum disulfide-water nanofluid flow*

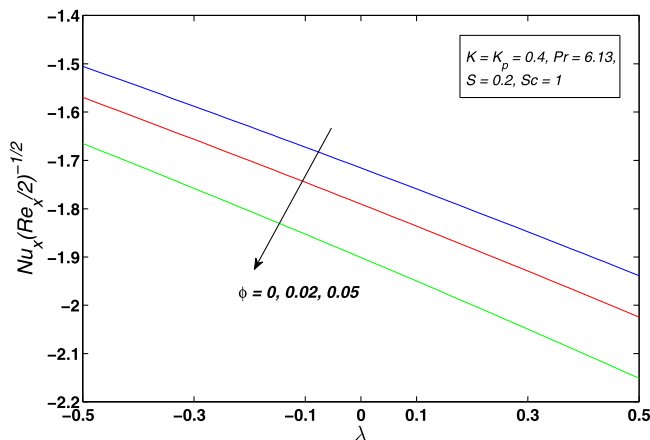


Fig. 15. (Color online) Impacts of  $\phi$  and  $\lambda$  on  $(Re_x/2)^{-1/2}Nu_x$ .

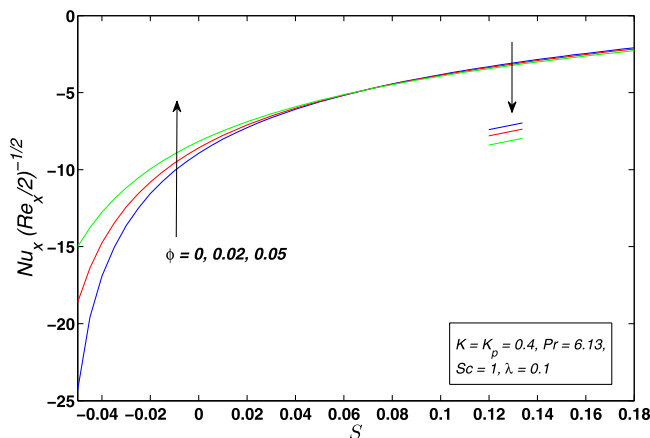


Fig. 16. (Color online) Impacts of  $\phi$  and suction and blowing on  $(Re_x/2)^{-1/2}Nu_x$ .

blowing. For higher suction heat transport rate is lower for the nanofluid than the regular fluid and for lower suction and blowing cooling of nanofluid is faster than the base fluid. Actually, high amount of suction sucks solid tiny-particles along with the base fluid causing the decay of heat transfer and the desired heat transport level is not achieved.

### 5. Concluding Notes with Recommendation for Further Works

Inspired by the applications of homogeneous-heterogeneous reaction in various industries, this work is devoted to the investigation of MoS<sub>2</sub>-water nanofluid flow over a vertical moving flat plate with combined effect of homogeneous-heterogeneous

chemical reactions, suction/blowing and mixed convection. The following are some key findings that might be summarised from this research:

- (a) Momentum and thermal layer thicknesses become thinner with suction and thicker with blowing. Temperature overshoot is higher for blowing case.
- (b) Enhanced homogeneous–heterogeneous reactions cause concentration boundary layer's thickness to rise.
- (c) Magnitude of surface-drag force decays and heat transport rate enhances with mixed convection.
- (d) Suction induces stronger drag-force and drops the speed of heat transport in magnitude.
- (e) For weaker suction and for blowing, cooling of nanofluid is faster, but contrast results are obtained for greater suction. Also, significant changes in heat transfer rate can be noted for blowing cases.


Lastly, it can be concluded for considered nanofluid flow that temperature overshoots are obtained for several controlling parameters, which affect the surface cooling rate. For highly mixed convection nature of the flow, we get desired situation, i.e. less drag with higher heat transfer rate. Our findings may be beneficial for many practical applications. In addition, with the view of the limitations of the study, the following points may be recommended for future considerations:


- (i) If quadratic term in mixed convection is considered in future investigation then may be some more important results can be witnessed.
- (ii) To generate more heat transfer efficiency, the flow medium can be taken as porous medium in a specific study.


## Acknowledgments


The authors are thankful to the anonymous reviewers for their helpful suggestions. K. Bhattacharyya also likes to acknowledge the support of “Faculty Incentive Grant” (No. R/Dev/D/IoE/Incentive/2022-23/47686) under IoE scheme of Banaras Hindu University.


## ORCID

Sohita Rajput  <https://orcid.org/0000-0001-7102-303X>

Krishnendu Bhattacharyya  <https://orcid.org/0000-0001-7975-0709>

Mitu Dular  <https://orcid.org/0009-0000-6341-1294>

Astick Banerjee  <https://orcid.org/0000-0001-6466-8171>

Ali J. Chamkha  <https://orcid.org/0000-0002-8335-3121>

## References

1. S. U. S. Choi, *Developments and Applications of Non-Newtonian Flows*, eds. D. A. Singer and H. P. Wang, FED-Vol. 231/MD-Vol. 66 (American Society of Mechanical Engineers, New York, 1995), pp. 99–105.
2. N. Bachok, A. Ishak and I. Pop, *J. Heat Transf.* **135**(5) (2013) 054501.
3. R. K. Tiwari and M. K. Das, *Int. J. Heat Mass Transf.* **50**(9–10) (2007) 2002.
4. O. D. Makinde and A. Aziz, *Int. J. Thermal Sci.* **50** (2011) 1326.
5. K. Das, *Heat Transf. Asian Res.* **42**(3) (2013) 230.
6. N. Acharya, K. Das and P. K. Kundu, *Alex. Eng. J.* **55** (2016) 1177.
7. K. Das, N. Acharya and P. K. Kundu, *Appl. Thermal Eng.* **103** (2016) 38.
8. N. Acharya, K. Das and P. K. Kundu, *Europ. Phys. J. Plus* **131** (2016) 303.
9. R. Dhanai, P. Rana and L. Kumar, *Powder Technology* **273** (2015) 62.
10. A. K. Verma, S. Rajput, K. Bhattacharyya and A. J. Chamkha, *Chem. Eng. J. Adv.* **12** (2022) 100366.
11. A. K. Verma, S. Rajput, K. Bhattacharyya, A. J. Chamkha and D. Yadav, *Chem. Eng. J. Adv.* **12** (2022) 100401.
12. M. Ibrahim, T. Saeed, F. R. Bani, S. N. Sedeh, Y.-M. Chu and D. Toghraie, *Powder Technol.* **384** (2021) 522.
13. Y. M. Chu, F. Shah, M. I. Khan, S. Kadry, Z. Abdelmalek and W. A. Khan, *J. Mater. Res. Technol.* **9**(6) (2020) 13977.
14. S. Z. Abbas, M. Waqas, A. Thaljaoui, M. Zubair, A. Riahi, Y. M. Chu and W. A. Khan, *Soft Comput.* **26** (2022) 1033.
15. M. Ashraf, A. Abbas, S. Zia, Y.-M. Chu, I. Khan and K. S. Nisar, *CMC-Comput. Mater. Contin.* **65**(2) (2020) 1809.
16. J. K. Madhukesh, R. N. Kumar, R. P. Gowda, B. C. Prasannakumara, G. K. Ramesh, M. I. Khan, S. U. Khan and Y.-M. Chu, *J. Mol. Liq.* **335** (2021) 116103.
17. L. A. Lund, Z. Omar, S. Dero, Y. Chu, I. Khan and K. S. Nisar, *Comput. Mater. Contin.* **66**(2) (2020) 1963.
18. M. Hamid, M. Usman, T. Zubair, R. U. Haq and W. Wang, *Int. J. Heat Mass Transf.* **124** (2018) 706.
19. M. Samadder, R. K. Ray and D. Sanpui, *Ind. J. Phys.* **97** (2023) 1811.
20. M. K. Narayanaswamy, J. Kandasamy and S. Sivanandam, *Math. Comput. Appl.* **27**(6) (2022) 110.
21. J. H. Merkin, *Math. Comput. Model.* **24** (1996) 125.
22. P. K. Kameswaran, S. Shaw, P. Sibanda and P. V. S. N. Murthy, *Int. J. Heat Mass Transf.* **57** (2013) 465.
23. R. Nandkeolyar, P. K. Kameswaran, S. Shaw and P. Sibanda, *J. Heat Transf.* **136**(12) (2014) 122001.
24. M. Das, B. K. Mahatha and R. Nandkeolyar, *Proc. Eng.* **127** (2015) 1018.
25. M. Ramzan, A. Rafiq, J. D. Chung, S. Kadry and Y. M. Chu, *Sci. Rep.* **10**(1) (2020) 18339.
26. T. Hayat, M. Farooq and A. Alsaedi, *AIP Adv.* **5** (2015) 027130.
27. A. Zaib, A. Banerjee and K. Bhattacharyya, *Proc. Instit. Mech. Eng. Part E: J. Process Mech. Eng.* **232**(5) (2018) 566.
28. C. S. Sravanthi, F. Mabood, S. G. Nabi and S. A. Shehzad, *Propuls. Power Res.* **11**(2) (2022) 265.
29. Z. Abbas, I. Mehdi, J. Hasnain, A. K. Alzahrani and M. Asma, *Case Stud. Thermal Eng.* **42** (2023) 102718.
30. M. A. Chaudhary and J. H. Merkin, *Fluid Dyn. Res.* **16** (1995) 311.

A. K. Pandey et al.

31. S. Rajput, K. Bhattacharyya, A. K. Pandey and A. J. Chamkha, *JCIS Open* **8** (2022) 100064.
32. A. K. Gautam, S. Rajput, K. Bhattacharyya, A. K. Pandey, A. J. Chamkha and M. Begum, *Chem. Eng. J. Adv.* **12** (2022) 100365.
33. A. K. Pandey, K. Bhattacharyya, A. K. Gautam, S. Rajput, M. S. Mandal, A. J. Chamkha and D. Yadav, *Propuls. Power Res.* **12**(1) (2023) 153.
34. A. K. Pandey, S. Rajput, K. Bhattacharyya, A. J. Chamkha and D. Yadav, *Forces Mech.* **11** (2023) 100179.
35. S. Rajput, K. Bhattacharyya, A. K. Pandey and A. J. Chamkha, *Res. Eng.* **19** (2023) 101380.
36. M. K. Mohamed, N. A. Z. Noar, M. Z. Salleh and A. Ishak, *J. Appl. Fluid Mech.* **9**(5) (2016) 2369.